Preliminary investigation of the impact of Axial Ring Splitting on Image Quality for the Cost Reduction of Total-Body PET

N. Efthimiou, *Member IEEE*, A.C. Whitehead, *Student Member IEEE*, M. Stockhoff, *Student Member IEEE*, C. Thyssen, *Student Member IEEE*, S.J. Archibald and S. Vandenberghe, *Senior Member IEEE*

***Abstract*—Recently, the first TB-PET scanner was unveiled and the initial results were nevertheless impressive. However, the cost of a TB-PET scanner is prohibiting for many institutions around the globe. Therefore here we investigate a cost reduction strategy incorporating a flexible detector arrangement. The proposed arrangement increases the axial field of view while keeping the overall cost at lower levels. We propose the axial ring splitting, which separates the full rings, of a compact PET scanner, to an expanded scanner with rings having only even or only odd numbered detectors. In this paper some preliminary performance results using Monte Carlo simulations, will be presented. In this comparison three configurations were considered (a) full rings PET (b) half-split rings TB-PET (c) full-split rings TB-PET. In addition in this investigation the effects of a varying coincidence window are demonstrated. The preliminary results suggest that Config.A demonstrated the highest Noise Equivalent count rate using either a fixed or a varying coincidence window. The main reasons were the absence of gaps and better handling of background radiation. However, reconstructed images for a single bed, from a whole body acquisition, suggested that due to the longer single bed acquisition of the full-split rings geometry the images present better noise properties.**

I. Introduction

TOTAL-BODY Positron Emission Tomography (TB-PET) due to its high sensitivity addresses a long standing issue in PET imaging. The feature of this type of scanners is the long axial Field Of View (aFOV), designed with the aim of imaging large portions of the body without bed movement [1], [2]. The scientific interest in the novel imaging possibilities and technological challenges, has been surging. Finally, last year, the first commercial TB-PET scanner for human scanning was presented and the first scans reported [3], [4].

TB-PET scanners allow simultaneous imaging of distant organs, adding the possibility of investigating their mutual interactions. Other key areas include fast kinetics, injection of high activities of short-lived isotopes and the possibility of paediatric applications.

In this preliminary investigation three different TB-PET geometries, targeted for cost efficiency, were compared in terms of Noise Equivalent Count Rate (NECR) and qualitative image quality.

Manuscript received February 4, 2019. This project is supported by the European Cooperation for Science, Technology Action TD1401: Fast Advanced Scintillation Timing. NE and SJA would like to thank Dr. Assem Allam and his family for the generous donation to help found the PET Research Centre at the University of Hull and for their continued support. This project was supported in part by the Daisy Appeal Charity. We acknowledge the Viper High Performance Computing facility of the University of Hull and its support team.

A.C. Whitehead is supported by GE Healthcare.

N. Efthimiou and S. J. Archibald are with the PET research centre, Faculty of Health Sciences, University of Hull, Hull, HU6 7RX, UK (email: n.efthymiou@hull.ac.uk).

A. C. Whitehead is with the Institute of Nuclear Medicine, University College London, London, NW1 2BU, UK (email: alexander.whitehead.18@ucl.ac.uk).

M. Stockhoff is with the Medical Image and Signal Processing (MEDISIP), Ghent University, Ghent, Belgium (email: mariele.stockhoff@ugent.be).

C. Thyssen is with the Medical Image and Signal Processing (MEDISIP), Ghent University, Ghent, Belgium

S. Vandenberghe is with the Medical Image and Signal Processing (MEDISIP), Ghent University, Ghent, Belgium (email: Stefaan.Vandenberghe@UGent.be).

II. Materials and Methods

A. Simulation

The simulations were performed using GATE (v.8.1) [5] Monte Carlo simulation toolbox. The proposed TB-PET geometries were based on LYSO:Ce (LYSO) crystal blocks with 8×8 elements. Each LYSO pixel had size $4\times4\times20$ mm^3. The digitizer that was used came from a simulation model validated for the Philips Vereos scanner, from previously published measurements [6]. The energy resolution was set to 11.4% and a common energy window of $450-650$ keV was applied on the singles.

All simulated TB-PET scanner geometries had inner ring radius of 383 mm and each full ring had 512 detectors. With regards to the ring splitting (*chessboard* configurations) three geometries were considered:

- Compact (Config.A): axial length: 700 mm
- Half split (Config.B): axial length: 1050 mm
- Full split (Config.C): axial length: 1400 mm

The geometries under investigation are illustrated at Fig. 4.

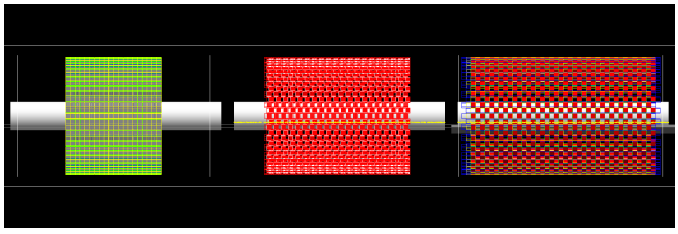

Fig. 1: Overview of the geometries considered in this study. In the order: Config.A, Config.B and Config.C.

In long PET geometries, acceptance of very oblique Line of Response (LOR) is not advised, as those γ-photons are attenuated intensively on the scanning body, reducing their benefits, while on the other hand the fraction of background events is increased.

Therefore the application of an axial limiting angle (θ_{max} has been proposed, in order to define the maximum accepted segment. In this study two axial limiting angles of $45\,\mathrm{deg}$ and $22.5\,\mathrm{deg}$, were considered. Due to the long aFOV a fixed coincidence window leads to sub-optimal results.

First, a typical coincidence window (4.5 ns), was considered. In this case coincidences of γ-photons detected at detectors more than approx. 23 cm apart are automatically rejected. Photon traveling in the crystal and timing resolution can affect this approximation. However if the window is extended further to accommodate larger detector differences, then the influx of randoms in the smaller segments is significantly increased.

The solution is the use of a varying coincidence window. In this case, the duration of the window depends on the segment number. In this study the window duration was set to 3.1 for direct sinograms and reached up to 9 ns for the extremities. We were allowed to use such a narrow coincidence window, as it can accommodate the active transverse Field Of View (FOV) of the direct planes. The modification was done directly on the GATE simulation toolkit.

B. Count losses

For the investigation of the count performance of the scanner the *Count losses* section of the NEMA protocol, was followed [7]. However, in order to better accommodate the long geometries of this study the typical 700 mm long NEMA scatter phantom was extended to 2000 mm. The simulations were performed for a single bed position.

C. Anthropomorphic XCAT phantom

The Anthropomorphic XCAT phantom [8] was simulated for 10 sec acquisition for a whole body acquisition.

The simulations were performed for a single bed position. Config.A needed three bed positions in order to cover the full body, therefore the acquisition time was reduced to a third, Config.B needed two bed positions and Config.C acquired the whole body with a single bed position for the full time.

D. Image reconstruction

The image reconstruction was performed using a modified version of STIR reconstruction toolkit [9].

The reconstructions were done with listmode (LM) Ordered Subsets-Expectation Maximisation (OSEM) algorithm, using 12 subsets for 2 full iterations. In the reconstructions only true events were used. Attenuation and normalisation (geometric effects) were applied. The normalisation coefficients were in particularly crucial due to gaps (*chessboard* effect) in the data [10]. Only single bed positions were reconstructed. In all cases, a 2 mm post-reconstruction Gaussian filter was applied on the reconstructed images.

For the reconstruction of the longest configuration (Config.C). the unstable STIR (pre v.4), downloaded from https://github.com/UCL/STIR was modified to handle memory in a more efficient way.

III. Results and Discussion

A. Count rates with fixed coincidence window

The NECR curves of the three configurations with the application of the constant coincidence window (4.5 ns), are shown on Fig. 2.

As the preliminary results suggest the compact geometry (Config.A) has higher counting performance than the split configurations. The presence of the gaps strongly reduces the sensitivity of the system, even after elongating the phantom.

Even without the presence of an axial limiting angle. The relatively small coincidence window does not allow the γ-photons on very oblique LORs to be detected, limiting the potential benefits of the longer scanning area.

The impact of the limiting angle is negligible for Config.A, due to geometrical reasons. On the other hand, its effect on the long geometries is limited due to the short coincidence window 4.5 ns which effectively rejects long distance γ-photons.

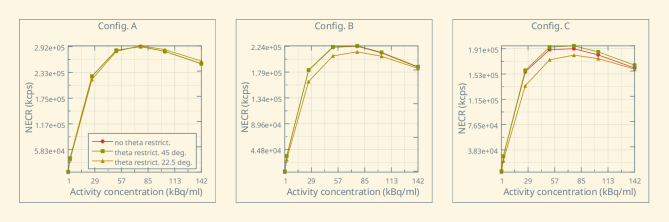

Fig. 2: NECR curves for the three configuration, constant coincidence window and two axial limiting angles $45\,\mathrm{deg}$ and $22.5\,\mathrm{deg}$

B. Effect of varying coincidence window

Using the modified GATE toolkit the effect of a varying coincidence window was investigated. The results showed (Fig. 3) that the NECR was strongly improved for all cases, 13%, 25% and 50% for Config.A, Config.B and Config.C, respectively. However, the compact geometry again demonstrated the highest counting performance.

The compact geometry even under this configuration, has lowest rate of background influx. In addition, it has the highest prompts influx as there are not gaps in the direct or small segments (which have the lowest attenuation).

C. Image reconstruction

In terms of image reconstruction, we can see that the modified STIR is able to reconstruct data from very long PET scanners.

In terms of qualitative image quality, the images suggest that the longer scanning time (10 sec) for the extended (Config.C) scanner provided images with better noise properties, than the more sensitive compact geometries.

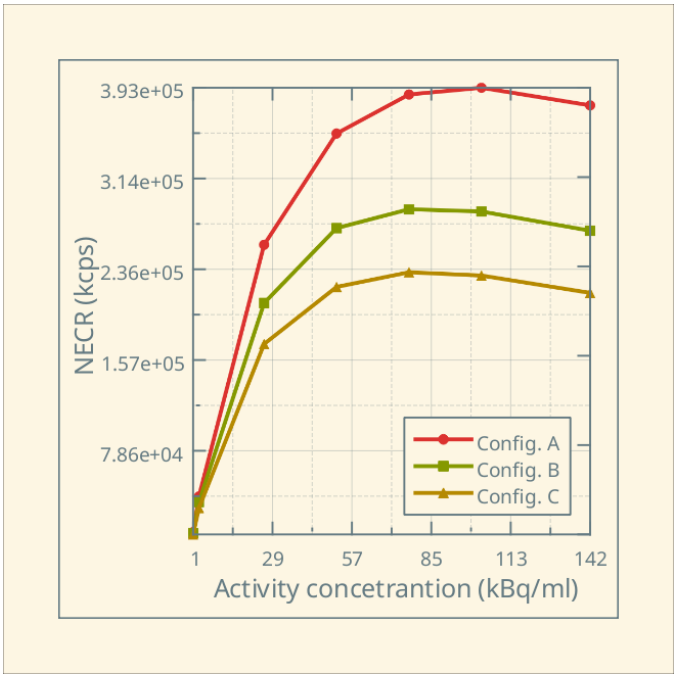

Fig. 3: NECR curves for the three configuration, with a varying coincidence window.

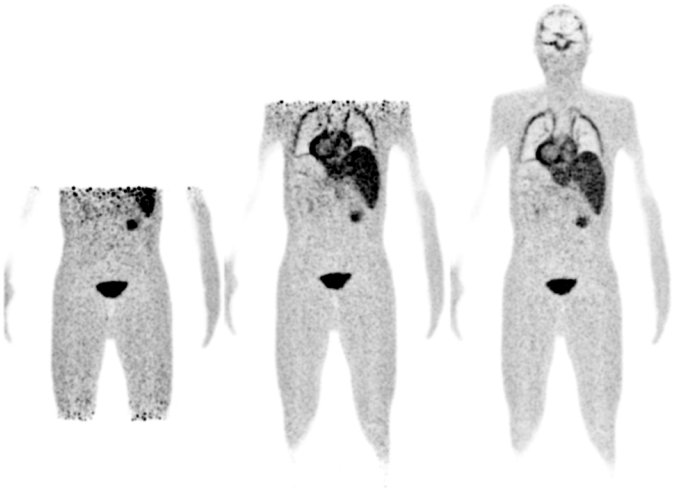

Fig. 4: Reconstructed images of the three long axial FOV PET geometries, after 2 full iterations using OSEM with 12 subsets.

IV. Conclusion

In this preliminary study the performance of a split-ring (*chessboard*) PET scanner was assessed and compared to a compact geometry, with the same total number of detectors.

This study was performed using GATE Monte Carlo simulations. The GATE (v8.0) was modified to provide a varying coincidence window from 3.1 ns for direct sinograms up to 9 ns for the extreme cases.

In terms of NECR the compact geometries perform better, due to the lack of gaps, better background photons handling and less attenuation. The application of the varying coincidence window strongly improves the NECR.

Reconstructed images from simulations of the anthropomorphic XCAT phantom for a single bed position, showed that even with the smaller NECR the split geometry is able to provide images with better noise properties. The reason is that the scanner acquired data for the total acquisition time.

V. Future work

Thanks to STIR's, modular structure, all other features present in the library such as Time-of-Flight reconstruction [11], [12], regularised reconstruction [13]–[16], scatter [17], [18], motion correction [19], [20] and parametric imaging [21], resolution recovery [22] e.t.c., would be immediately available for Total Body PET scanners.

References

[1] S. R. Cherry, T. Jones, J. S. Karp, J. Qi, W. W. Moses, and R. D. Badawi, "Total-Body PET: Maximizing Sensitivity to Create New Opportunities for Clinical Research and Patient Care." *J. Nucl. Med.*, vol. 59, no. 1, pp. 3–12, 2018.

[2] P. Moskal, D. Kisielewska, C. Curceanu, E. Czerwiński, K. Dulski, A. Gajos, M. Gorgol, B. Hiesmayr, B. Jasińska, K. Kacprzak, Kapłon, G. Korcyl, P. Kowalski, W. Krzemień, T. Kozik, E. Kubicz, M. Mohammed, S. Niedźwiecki, M. Pałka, M. Pawlik-Niedźwiecka, L. Raczyński, J. Raj, S. Sharma, Shivani, R. Y. Shopa, M. Silarski, M. Skurzok, E. Stępień, W. Wiślicki, and B. Zgardzińska, "Feasibility study of the positronium imaging with the J-PET tomograph," *Phys. Med. Biol.*, vol. 64, no. 5, p. 055017, 3 2019.

[3] E. K. Leung, M. S. Judenhofer, S. R. Cherry, and R. D. Badawi, "Performance assessment of a software-based coincidence processor for the EXPLORER total-body PET scanner," *Phys. Med. Biol.*, vol. 63, no. 18, p. 18NT01, 9 2018.

[4] R. D. Badawi, H. Shi, P. Hu, S. Chen, T. Xu, P. M. Price, Y. Ding, B. A. Spencer, L. Nardo, W. Liu, J. Bao, T. Jones, H. Li, and S. R. Cherry, "First Human Imaging Studies with the EXPLORER Total-Body PET Scanner." *J. Nucl. Med.*, vol. 60, no. 3, pp. 299–303, 3 2019.

[5] S. Jan, G. Santin, D. Strul, S. Staelens, K. Assié, D. Autret, S. Avner, R. Barbier, M. Bardiès, P. M. Bloomfield, D. Brasse, V. Breton, P. Bruyndonckx, I. Buvat, A. F. Chatziioannou, Y. Choi, Y. H. Chung, C. Comtat, D. Donnarieix, L. Ferrer, S. J. Glick, C. J. Groiselle, D. Guez, P.-F. Honore, S. Kerhoas-Cavata, A. S. Kirov, V. Kohli, M. Koole, M. Krieguer, D. J. v. d. Laan, F. Lamare, G. Largeron, C. Lartizien, D. Lazaro, M. C. Maas, L. Maigne, F. Mayet, F. Melot, C. Merheb, E. Pennacchio, J. Perez, U. Pietrzyk, F. R. Rannou, M. Rey, D. R. Schaart, C. R. Schmidtlein, L. Simon, T. Y. Song, J.-M. Vieira, D. Visvikis, R. V. d. Walle, E. Wieërs, and C. Morel, "GATE: a simulation toolkit for PET and SPECT," *Phys. Med. Biol.*, vol. 49, no. 19, pp. 4543–4561, 10 2004.

[6] I. Rausch, A. Ruiz, I. Valverde-Pascual, J. Cal-González, T. Beyer, and I. Carrio, "Performance Evaluation of the Vereos PET/CT System According to the NEMA NU2-2012 Standard," *J. Nucl. Med.*, vol. 60, no. 4, pp. 561–567, 4 2019.

[7] National Electrical Manufacturers Association, *Performance measurements of positron emission tomographs. NEMA Standards Publication NU 2-2012*, 2012.

[8] W. P. Segars, G. Sturgeon, S. Mendonca, J. Grimes, and B. M. W. Tsui, "4D XCAT phantom for multimodality imaging research," *Med. Phys.*, vol. 37, no. 9, p. 4902, 2010.

[9] K. Thielemans, C. Tsoumpas, S. Mustafovic, T. Beisel, P. Aguiar, N. Dikaios, and M. W. Jacobson, "STIR: software for tomographic image reconstruction release 2," *Phys. Med. Biol.*, vol. 57, no. 4, pp. 867–883, 2 2012.

[10] T. Niknejad, S. Tavernier, J. Varela, and K. Thielemans, "Validation of 3D model-based Maximum-Likelihood estimation of normalisation factors for partial ring Positron Emission Tomography," in *2016 IEEE Nuclear Science Symposium, Medical Imaging Conference and Room-Temperature Semiconductor Detector Workshop, NSS/MIC/RTSD 2016*, vol. 2017-January. Institute of Electrical and Electronics Engineers Inc., 10 2017.

[11] N. Efthimiou, E. Emond, P. Wadhwa, C. Cawthorne, C. Tsoumpas, and K. Thielemans, "Implementation and validation of time-of-flight PET image reconstruction module for listmode and sinogram projection data in the STIR library," *Phys. Med. Biol.*, vol. 64, no. 3, p. 035004, 1 2019.

[12] P. Wadhwa, K. Thielemans, N. Efthimiou, K. Wangerin, T. Deller, G. Delso, N. Keat, D. Deidda, E. Emond, M. Tohme, F. Jansen, R. Gunn, D. Buckley, W. Hallett, and C. Tsoumpas, "PET Image reconstruction using physical and mathematical modelling for time of flight PET-MR scanners in the STIR library," *Methods (in press)*.

[13] M. J. Ehrhardt, K. Thielemans, L. Pizarro, D. Atkinson, S. Ourselin, B. F. Hutton, and S. R. Arridge, "Joint reconstruction of PET-MRI by exploiting structural similarity," *Inverse Problems*, vol. 31, no. 1, p. 015001, 1 2015.

[14] K. Karaoglanis, I. Polycarpou, N. Efthimiou, and C. Tsoumpas, "Appropriately regularized OSEM can improve the reconstructed PET images of data with low count statistics," *Hellenic Journal of Nuclear Medicine*, vol. 18, no. 2, pp. 140–145, 6 2015.

[15] D. Deidda, N. Efthimiou, R. Manber, K. Thielemans, P. Markiewicz, R. Aykroyd, and C. Tsoumpas, "Comparative evaluation of image reconstruction methods for the Siemens PET-MR scanner using the STIR library," in *2016 IEEE Nuclear Science Symposium, Medical Imaging Conference and Room-Temperature Semiconductor Detector Workshop, NSS/MIC/RTSD 2016*, vol. 2017-Janua, 2017.

[16] D. Deidda, N. A. Karakatsanis, P. M. Robson, Y.-J. Tsai, N. Efthimiou, K. Thielemans, Z. A. Fayad, R. G. Aykroyd, and C. Tsoumpas, "Hybrid PET-MR list-mode kernelized expectation maximization reconstruction," *Inverse Problems*, vol. 35, no. 4, p. 044001, 4 2019.

[17] L. Brusaferri, A. Bousse, N. Efthimiou, E. Emond, D. Atkinson, S. Ourselin, B. F. Hutton, S. Arridge, and K. Thielemans, "Potential benefits of incorporating energy information when estimating attenuation from PET data," in *2017 IEEE Nuclear Science Symposium and Medical Imaging Conference (NSS/MIC)*. IEEE, 10 2017, pp. 1–4.

[18] L. Brusaferri, A. Bousse, Y.-J. Tsai, D. Atkinson, S. Ourselin, B. F. Hutton, S. Arridge, and K. Thielemans, "Maximum-likelihood estimation of emission and attenuation images in 3D PET from multiple energy window measurements," in *2018 IEEE Nuclear Science Symposium and Medical Imaging Conference Proceedings (NSS/MIC)*. IEEE, 11 2018, pp. 1–3.

[19] R. Manber, K. Thielemans, B. F. Hutton, A. Barnes, S. Ourselin, S. Arridge, C. O'Meara, S. Wan, and D. Atkinson, "Practical PET Respiratory Motion Correction in Clinical PET/MR," *Journal of Nuclear Medicine*, vol. 56, no. 6, pp. 890–896, 6 2015.

[20] A. Gillman, J. Smith, P. Thomas, S. Rose, and N. Dowson, "PET motion correction in context of integrated PET/MR: Current techniques, limitations, and future projections," *Medical Physics*, vol. 44, no. 12, pp. e430–e445, 12 2017.

[21] R. Brown, B. A. Thomas, A. Rashidnasab, K. Erlandsson, E. Ovtchinnikov, E. Pasca, A. Reader, J. C. Matthews, C. Tsoumpas, and K. Thielemans, "Motion-corrected reconstruction of parametric images from dynamic PET data with the Synergistic Image Reconstruction Framework (SIRF)," in *2018 IEEE Nuclear Science Symposium and Medical Imaging Conference Proceedings (NSS/MIC)*. IEEE, 11 2018, pp. 1–4.

[22] E. C. Emond, A. M. Groves, B. F. Hutton, and K. Thielemans, "Effect of positron range on PET quantification in diseased and normal lungs," *Physics in Medicine & Biology*, vol. 64, no. 20, p. 205010, 10 2019.